JMEPEG (2012) 21:1772–1776
DOI: 10.1007/s11665-011-0080-4

1059-9495/$19.00

Eddy Current Assessment of the Cold Rolled Deformation Behavior of AISI 321 Stainless Steel

Kunpeng Liu, Zihua Zhao, and Zheng Zhang

(Submitted March 11, 2011; in revised form October 29, 2011)

Applicability of the eddy current (EC) technique in assessing martensite phase transformation during cold reduction in AISI 321 stainless steel was investigated. An empirical model based on measured EC parameters was developed for predicting the volume fraction of strain-induced martensite. Good agreement was found between the model-predicted and the experimental data.

Keywords cold rolling, eddy current, strain-induced martensite, Vickers hardness, X-ray diffraction

1. Introduction

Austenite stainless steel is widely used because of its toughness, plasticity, and good corrosion resistance (Ref 1). Single-phase austenite steel is paramagnetic, and a new ferromagnetic alpha′ phase can form after cold working. The alpha′ phase produced is often called strain-induced martensite because it originates from diffusionless phase transformation (Ref 2). The volume fraction of this type of martensite has a significant effect on its material properties (Ref 3).

AISI 321 stainless steel obtained from solution treatment features a fully austenitic microstructure. Strain-induced martensite can be formed in the austenite matrix during cold rolling. The volume fraction of martensite transformed can be measured by magnetic methods, X-ray (XRD) or neutron diffraction, and quantitative metallography, among others (Ref 4-6). The eddy current (EC) technique, which reveals the electromagnetic properties of materials, is sensitive to strain-induced martensite in austenite matrices. However, it is rarely used compared with other magnetic methods.

In 1992, Habiby (Ref 7) measured the volume fraction of the austenite in maraging steel using the EC technique, and discovered that it was suitable for the rapid and quantitative determination of the austenite phase. Especially, EC technique could be applied on the production floor with relative ease compared to the X-ray method. Some reports also showed that the EC technique could measure the strain-induced martensite of austenite stainless steel under low cycle fatigue (Ref 8-10). In 2006, Lois (Ref 11) established a linear relationship between calculated EC parameters (reactance and resistance) and the alpha′-martensite content of AISI 347 steel with heat treatment at different temperatures after cold rolling; the slope found was opposite that of the reactance and resistance lines. This result showed that it is difficult to conduct EC evaluations without transformation of experimental output data. In 2008, Khan (Ref 12) recorded the EC parameters of a series of cold rolled austenite stainless steel specimens, and showed that it was useful for characterizing the volume fraction of martensite during cold reduction. However, the relationship between the hardness and EC parameters was not observed, and the correlation coefficient of linear fitting between the austenite percentage and the EC parameter was low.

The present study seeks to establish the relationship between strain-induced martensite and the EC parameters of cold rolled AISI 321 steel. XRD was conducted to measure the volume fraction of alpha′-martensite obtained from cold rolling. The effect of cold reduction was examined based on the eddy current array (ECA) and Vickers hardness of the specimen.

2. Experimental Procedures

The specimens used in this work were obtained from one batch of AISI 321 alloy. The chemical composition of the materials is shown in Table 1. Specimens measuring 90 mm × 20 mm × 5.5 mm were deformed by cold rolling to within 0-70% reduction at room temperature. These deformed specimens were examined using Vickers hardness test. The volume fraction of strain-induced martensite was measured by XRD. An OmniScan ECA measurement system, with an absolute surface probe (SBBR-025-01M-032) with a frequency range of 300-3000 kHz, was used in this work. The instrument was calibrated using a specimen without cold rolling; other specimens were tested using this calibration. The results of EC amplitude represent the average value of three measurements over a region of the test piece.

The ECA probe (SBBR-025-01M-032) is absolute bridge double row probe, which contains 32 coils with diameter of 0.8 and 25 mm coverage. Every coil is one individual EC probe, and the magnetic field interference of adjacent coils is shield by exciting at different time slot. The signal processing system can received every coil signal and display the maximum signal of

Electronic supplementary material The online version of this article (doi:10.1007/s11665-011-0080-4) contains supplementary material, which is available to authorized users.

Kunpeng Liu, Zihua Zhao, and **Zheng Zhang**, Key Laboratory of Aerospace Materials and Performance (Ministry of Education), School of Materials Science and Engineering, Beihang University, Beijing, China. Contact e-mail: zhangzh@buaa.edu.cn.

Table 1 Chemical composition of AISI 321 stainless steel (wt.%)

Alloy	Si	Ni	Mn	Ti	Cr	C	S	Fe
AISI 321	0.714	9.15	1.45	0.452	17.550	0.0523	0.021	Balance

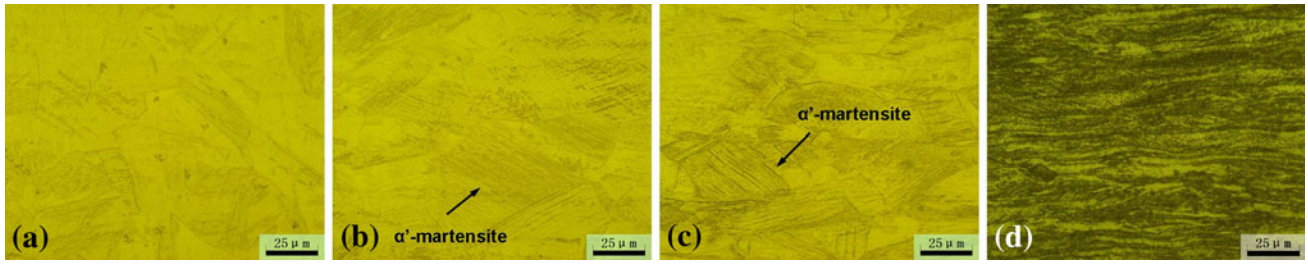

Fig. 1 The microstructure of AISI 321 stainless steel with different cold reductions: (a) 0%, (b) 17.88%, (c) 36.20%, (d) 70.3%

them. During measurement, the probe drive voltage is 1.0 V; the frequency range is 500-2500 kHz.

3. Results and Discussion

3.1 Microstructure

The specimens were polished and etched with a mixture of nitric acid, hydrochloric acid, and water (10:10:1), and then examined using an optical microscope (BX51M). The microstructures of AISI 321 stainless steel specimens subjected to different cold reductions are shown in Fig. 1. The grains are elongated and the strain-induced martensite phase can be seen after cold rolling.

3.2 Hardness and XRD

The Vickers hardness (HV) of specimens subjected to different cold reductions was measured to assess their mechanical properties. The curve in Fig. 2 shows that the hardness increased continuously with increasing cold reduction, but the rate of increase gradually slowed. Bigdeli Karimi (Ref 4) explained that the increasing rate of hardness is reduced as a result of the reduction in the rate of martensite formation.

XRD was conducted using Cu Kα radiation. Typical XRD spectra obtained from specimens subjected to different cold reductions are shown in Fig. 3. The specimen without cold reduction was fully austenitic; austenite peak intensities gradually decreased and martensite peaks appeared with steadily increasing intensities with increasing cold reduction. The volume fraction of alpha′-martensite at each step was calculated using formula (I) (Ref 13):

$$\frac{V_M}{V_M + V_A} = \frac{I_M/R_M}{I_M/R_M + A_A/R_A} \quad \text{(Eq I)}$$

where V_i, I_i, and R_i, are, respectively, the volume, integrated intensity, and intensity factor of a certain phase, and the subscripts M and A denote the strain-induced martensite and austenite phases, respectively.

The volume fraction of the strain-induced martensite for AISI 321 specimens with different cold reductions are shown in Fig. 2. The volume fraction of the strain-induced martensite increased with increasing cold reduction up to 70%. A dramatic difference was observed between the volume fraction of the strain-induced martensite and *HV* curves in Fig. 2. The martensite volume changed slightly, but the *HV* increased rapidly within 8% cold reduction. Plastic deformation of austenitic stainless steel during cold rolling resulted in the appearance of alpha′-martensite and increases in dislocation density. Thresholds exist for the formation of martensite as a function of accumulated plastic strain (Ref 9), but the increase in dislocation density was approximately synchronous with that of plastic strain. Thus, the increase in dislocation density was the main factor for the rapid increase in hardness at 8% cold reduction. However, martensite is the main hardening mechanism of austenite steel (Ref 1). Thus, the hardness and strain-induced martensite curves became more and more similar with increasing cold reduction. The relationship between the hardness and the volume fraction of strain-induced martensite under cold reductions between 8 and 70% is shown in Fig. 4. Figure 4 reveals that the hardness was proportional to the volume fraction of strain-induced martensite. Hence, the hardness of AISI 321 stainless steel can be expressed by the volume fraction of strain-induced martensite subjected to 8-70% cold reduction.

3.3 Eddy Current Measurements

EC measurements were conducted on polished specimens with good surface conditions. A standard specimen was chosen and the instrument was calibrated with it. The standard specimen used was a polished plate with no defects and no cold reduction. The calibration contained two variables, amplitude and phase. The amplitude of the sensor in air was calibrated to 5.000 V and the phase was 180°. The measured maximum amplitude of the calibrated EC probe reading A_{max} (the maximum amplitude vector) with different frequencies as a function of cold reduction are plotted in Fig. 5. It can be observed that the amplitudes curves of the EC at different frequencies are similar, i.e., slight changes within 8% cold reduction, sharp increases under 8-50% cold reduction, and slow increases within 50-70% cold reduction were observed. The amplitude decreased with increasing frequency from 500 to 2500 kHz. This phenomenon can be explained by the relation between the penetration depth of the EC and the exciting

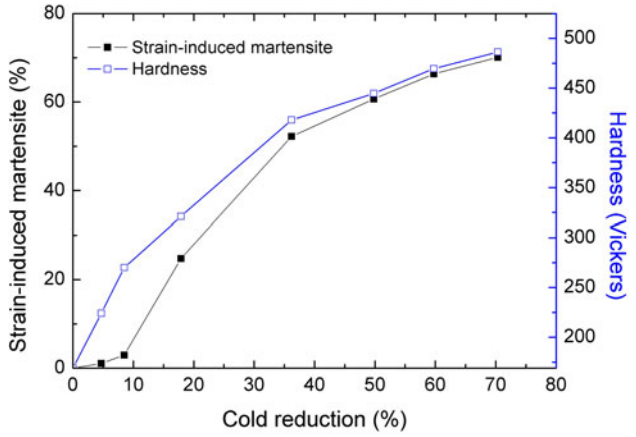

Fig. 2 Relation between the volume fraction of strain-induced martensite (or hardness) and cold reduction

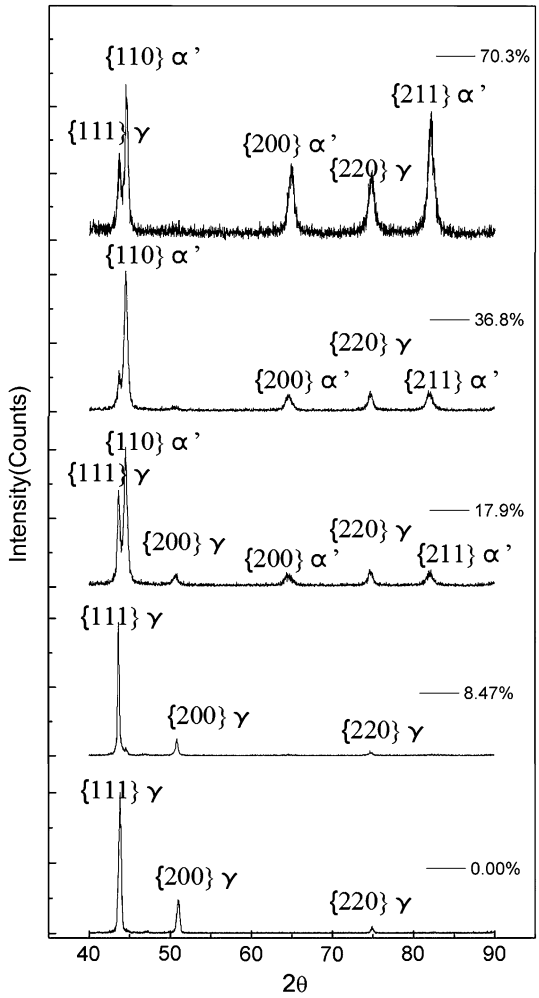

Fig. 3 Typical XRD spectra of specimens with different cold reductions

frequency. The standard penetration depth of the EC is inversely proportional to the square root of the frequency, so the standard penetration depth of the EC decreases with increasing frequency. Consequently, the higher the frequency, the lower the amplitude (A_{max}) obtained in this test.

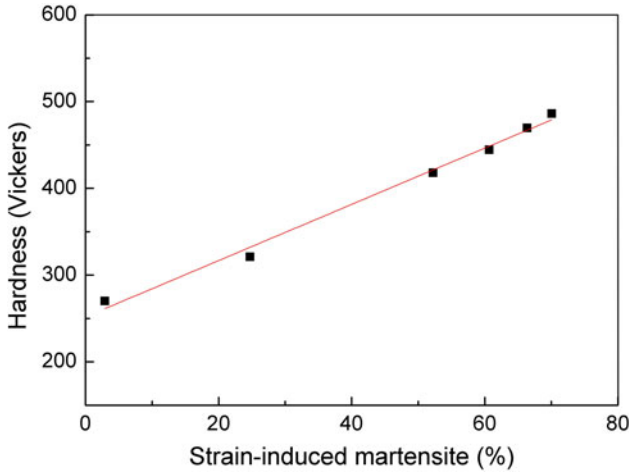

Fig. 4 Variation of hardness as a function of the volume fraction of strain-induced martensite

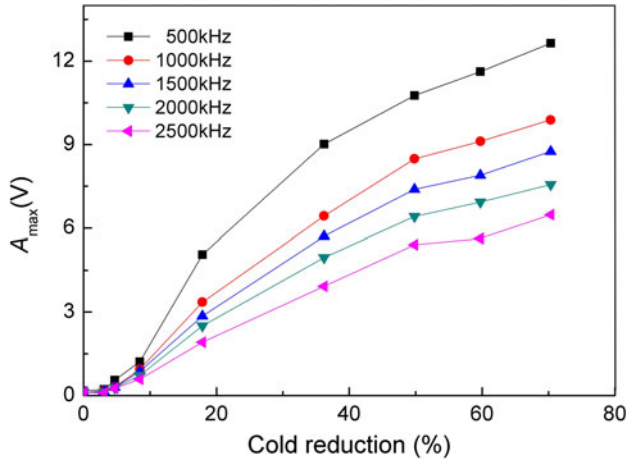

Fig. 5 The relation between A_{max} and cold reduction at different frequencies

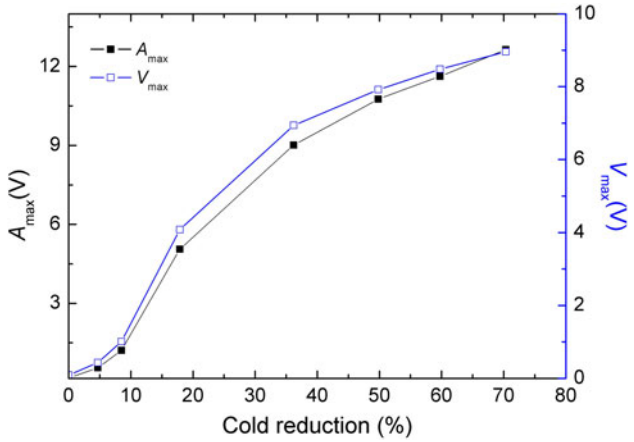

Fig. 6 The relation between A_{max} (or V_{max}) and cold reduction at 500 kHz

Generally, V_{max} (the vertical component of A_{max}) is applied to measure material defects because the phase of maximal lift off (amplitude in air) is calibrated in the horizontal direction, and the vertical component (V_{max}) can successfully eliminate the influence of lift off. The relation between A_{max} (or V_{max}) at 500 kHz and cold reduction is shown in Fig. 6. The trends of A_{max} and V_{max} are similar. Thus, the lift off effect could be ignored because of little influence on A_{max}. The effect of thickness had been considered in the measurement (Table S1, Supporting information). The result indicated that it was negligible too.

3.4 Establishment and Evaluation of the Eddy Current Predict Models of Ferromagnetic Martensite and Hardness

Most EC measurements are conducted in "impedance" mode. Relative to non-ferromagnetic materials, the coil impedance of ferromagnetic materials increases by one to two orders of magnitude. Ferromagnetic alpha′-martensite is the main contributor to the maximum amplitude (A_{max}) in this experiment, although the density of dislocation increases at the same time. Figure 7 shows the relationship between the A_{max} (or V_{max}) of the EC at 500 kHz and the volume fraction of martensite. A_{max} (or V_{max}) is proportional to the volume fraction of strain-induced martensite. Consequently, the prediction model of strain-induced martensite in cold rolled AISI 321 stainless steel can be expressed as:

$$M\% = -2.647 + 5.864 \times A_{max}, \quad R = 0.9985 \qquad \text{(Eq 1)}$$

$$M\% = -3.626 + 8.099 \times V_{max}, \quad R = 0.9967 \qquad \text{(Eq 2)}$$

where $M\%$ is the volume fraction of strain-induced martensite.

It was previously stated in "Hardness and XRD" section that the hardness is proportional to the volume fraction of strain-induced martensite volume beyond 8% cold reduction. Thus, there is a linear relation between the hardness and A_{max} (or V_{max}) within 8-70% cold reduction. The fitting results of the relationship between the hardness and A_{max} (or V_{max}) at 500 kHz within 8-70% cold reduction is shown in Fig. 8. The hardness can be described as follows:

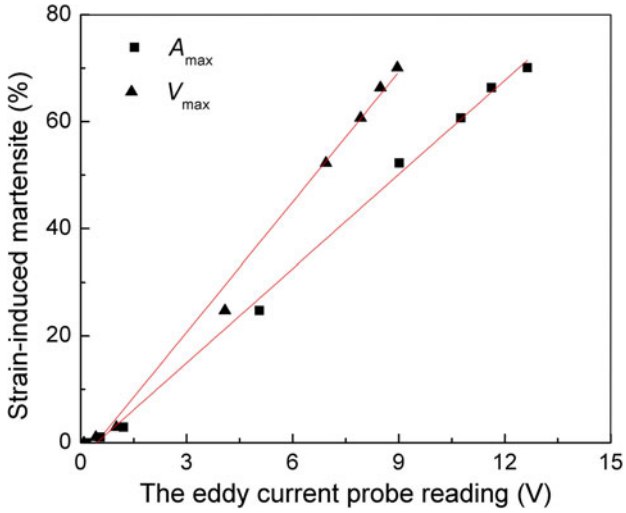

Fig. 7 The relation of the volume fraction of strain-induced martensite and A_{max} (or V_{max}) at 500 kHz

$$HV = 237.3 + 19.59 \times A_{max}, \quad R = 0.9938 \qquad \text{(Eq 3)}$$

$$HV = 228.3 + 27.81 \times V_{max}, \quad R = 0.9874 \qquad \text{(Eq 4)}$$

where HV is the Vickers hardness.

In order to verify the validity and stability of these prediction models, four specimens with different cold reductions were prepared. The relations between the A_{max} and V_{max} of the EC, the Vickers hardness, and the strain-induced martensite of these specimens were examined under the same experimental conditions as applied in previous analyses. The volume fraction of strain-induced martensite and the Vickers hardness were calculated by applying A_{max} into models (1) and (3) and V_{max} into models (2) and (4). The results are shown in Fig. 9 and 10. The predicted values are consistent with the experimental ones.

The relative errors (a_t) and the average absolute relative errors (AARE) of the models were calculated using formulas (II) and (III):

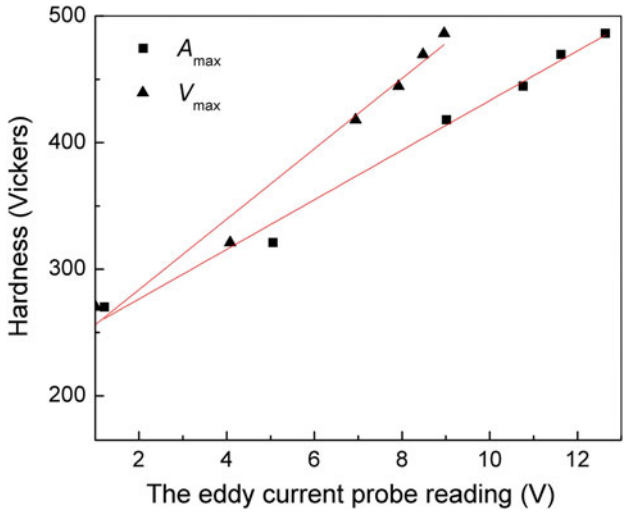

Fig. 8 The relation of hardness and A_{max} (or V_{max}) at 500 kHz

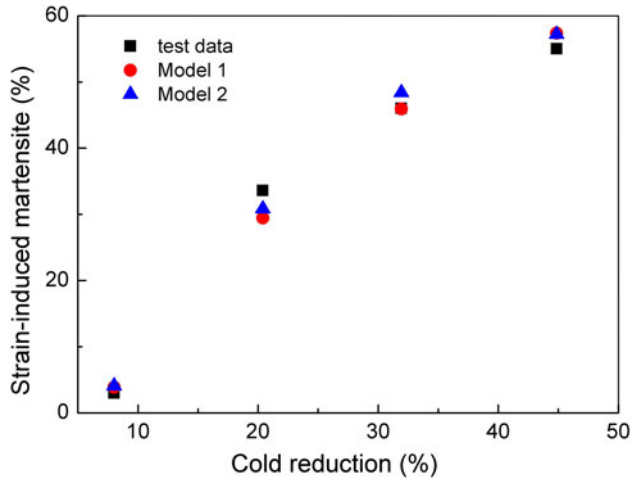

Fig. 9 The verified result of models (1) and (2)

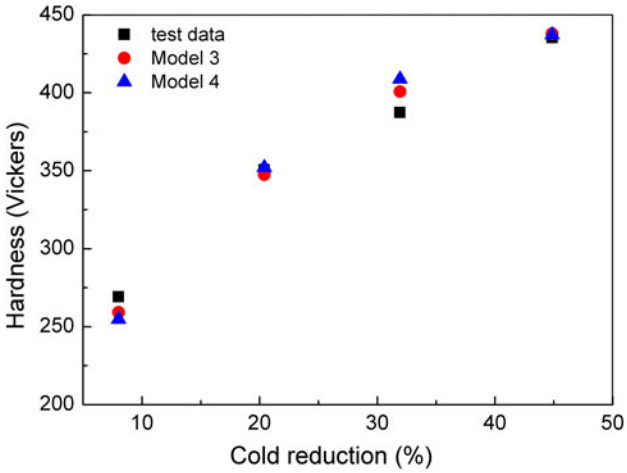

Fig. 10 The verified result of models (3) and (4)

Table 2 The calculated errors of all the models

	The relative error, %			
Cold reduction, %	**Model (1)**	**Model (2)**	**Model (3)**	**Model (4)**
8.01	−30.81	−36.97	3.72	5.35
20.40	12.26	8.23	0.89	−0.43
31.93	0.24	−5.18	−3.44	−5.52
44.87	−4.24	−3.95	−0.59	−0.43
AARE, %	11.89	13.58	2.16	2.93

$$a_t = \frac{y_t - y_t^{'}}{y_t} \qquad \text{(Eq II)}$$

$$\text{AARE} = \frac{1}{n}\sum_{t=1}^{n}\left|\frac{y_t - y_t^{'}}{y_t}\right| \qquad \text{(Eq III)}$$

where y_t is the test data, $y_t^{'}$ is the predicted value, and n is the number of predicted points.

The calculated results are shown in Table 2. The relative errors of models (1) and (2) decreased with increasing cold reduction, showing that the prediction accuracy of strain-induced martensite models improved with increasing cold reduction. The relative errors of the hardness models did not exhibit this phenomenon. The AARE of models (1) and (3) were lower than those of models (2) and (4). In this experiment, the accuracy of the models in relation to A_{max} was higher compared with the accuracy of the models in relation to V_{max}. This may be due to the fact that V_{max} is a vertical component of A_{max}, and the influence of the horizontal component of A_{max} produced by strain-induced martensite was ignored. Thus, the A_{max} of the EC is preferable when characterizing the strain-induced martensite of cold rolled AISI 321 stainless steel.

4. Conclusion

The volume fraction of strain-induced martensite and the hardness of cold rolled AISI 321 stainless steel can be estimated by the maximum amplitude (A_{max}) and the maximum vertical component (V_{max}) of ECs. A linear correlation existed between A_{max} (or V_{max}) and the volume fraction of the strain-induced martensite (or hardness). The evaluated stability of strain-induced martensite was higher than that of hardness, and the evaluated accuracy of strain-induced martensite in relation to A_{max} was better than that in relation to V_{max}. Accuracy further improved with increasing cold reduction.

References

1. J. Xiao, 不锈钢的金属学问题 (*The Metallurgical Problems of Stainless Steel*), 1 st ed., The Press of Metallurgy Industry, Beijing, 1983, p 282–288 (in Chinese).
2. I. Mészáros and J. Prohászka, Magnetic Investigation of the Effect of α'-Martensite on the Properties of Austenitic Stainless Steel, *J. Mater. Process. Technol.*, 2005, **16**, p 162–168
3. E. Nagy, V. Mertinger, F. Tranta, and J. Sólyom, Deformation Induced Martensitic Transformation in Stainless Steels, *Mater. Sci. Eng., A*, 2004, **378**, p 308–313
4. M. Bigdeli Karimi, H. Arabi, A. Khosravani, and J. Samei, Effect of Rolling Strain on Transformation Induced Plasticity of Austenite to Martensite in a High-Alloy Austenitic Steel, *J. Mater. Process. Technol.*, 2008, **203**, p 349–354
5. S.A. Atroshenko, Martensite Transformation in Metals Induced Shock Loading, *Mater. Sci. Eng., A*, 2004, **378**, p 293–298
6. A.K. De, D.C. Murdock, M.C. Mataya, J.G. Speer, and D.K. Matlock, Quantitative Measurement of Deformation-Induced Martensite in 304 Stainless Steel by X-ray Diffraction, *Scripta Mater.*, 2004, **50**(12), p 1445–1449
7. F. Habiby, T.N. Siddiqui, S.H. Khan, A. ul Haq, and A.Q. Khan, Austenite Determination by Eddy Current Measurements in a Maraging Steel, *NDT & E Int.*, 1992, **25**(3), p 145–146
8. M. Lang, J. Johnson, J. Schreiber, G. Dobmann, H.-J. Bassler, D. Eifler, R. Ehrlich, and U. Gampe, Cyclic Deformation Behaviour of AISI 321 Austenitic Steel and Its Characterization by Means of HTC-SQUID, *Nucl. Eng. Des.*, 2000, **198**, p 185–191
9. M. Grosse, M. Niffenegger, and D. Kalkhof, Monitoring of Low-Cycle Fatigue Degradation in X6CrNiTi18-10 Austenitic Steel, *J. Nucl. Mater.*, 2001, **296**, p 305–311
10. V. Zilberstein, K. Walrath, D. Grundy, D. Schlicker, N. Goldfine, E. Abramovici, and T. Yentzer, MWM eddy-current arrays for crack initiation and growth monitoring, *Int. J. Fatigue*, 2003, **25**, p 1147–1155
11. A. Lois and M. Ruch, Assessment of Martensite Content in Austenitic Stainless Steel Specimens by Eddy Current Testing, *Insight*, 2006, **48**(1), p 26–29
12. S.H. Khan, F. Ali, A. Nusair Khan, and M.A. Iqbal, Eddy Current Detection of Changes in Stainless Steel After Cold Reduction, *Comput. Mater. Sci.*, 2008, **43**(4), p 623–628
13. Q. Yang and J.L. Luo, Martensite Transformation and Surface Cracking of Hydrogen Charged and Outgassed Type 304 Stainless Steel, *Mater. Sci. Eng., A*, 2000, **288**(1), p 75–83